ACS APPLIED MATERIALS & INTERFACES

RESEARCH ARTICLE

www.acsami.org

A Gold Nanoparticle Platform for Protein−Protein Interactions and Drug Discovery

Andrew B. Thompson,[†] Amy K. Calhoun,[†] Benoit J. Smagghe,[†] Maria D. Stevens,[†,‡] Mark T. Wotkowicz,[†] Vasilios M. Hatziioannou,[†] and Cynthia Bamdad*[,†]

[†]Minerva Biotechnologies, 40 Bear Hill Road, Waltham, Massachusetts 02451, United States

[‡]Northeastern University, Boston, Massachusetts 02115, United States

Supporting Information

ABSTRACT: Gold nanoparticles hold great promise for studying protein−protein interactions because of their intrinsic optical properties. Pink when in a homogeneous suspension, the solution turns blue-gray when particles are drawn close together, for example, when immobilized proteins specifically interact with each other. However, the nanoparticle stability, size, and method of protein attachment contribute to the unreliable outcome of current assays. To overcome these hurdles, we developed novel and reliable methods first to synthesize homogenous particles of optimal diameter and second to apply a heterologous NTA-Ni-SAM coating for controlled orientation and optimal presentation of histidine-tagged proteins. Both methods were proven to greatly enhance assay sensitivity and specificity by increasing the signal and minimizing the nonspecific binding. Our assay reproducibly detected known protein−protein interactions and unambiguously identified small molecules that inhibited them. We believe our gold nanoparticle bioassay is a versatile and trustworthy new platform for analyzing protein−protein interactions and high-throughput screening of small-molecule inhibitors.

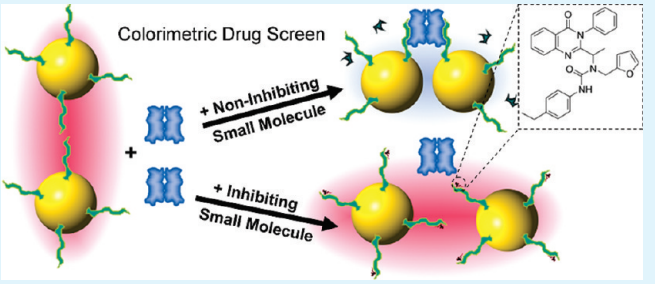

KEYWORDS: gold nanoparticles, drug screen, nitrilotriacetic acid, protein binding

INTRODUCTION

Protein−protein interactions are the core of the signal transduction pathways that control and regulate major cellular processes required for vital biological functions.[1,2] Such a critical role has driven the development of a multitude of methods to analyze the molecular aspects of those binding events. Each method possesses certain limitations, most notably in the areas of sensitivity and specificity, that have been difficult to overcome using a single method. In addition, current assays often rely on indirect methods requiring fastidious labor, time-consuming labeling procedures, and expensive equipment.[3−5]

Gold nanoparticles (AuNPs) have unique properties that make them a very attractive research tool for a wide variety of disciplines,[6,7] including solution-based bioassays. More specifically, AuNPs used for the study of protein−protein interactions could overcome the limits of current methods. AuNPs are spherical, are chemically inert, possess an inherent optical signaling capability, and are amenable to convenient thiol-based surface chemistries. Colloidal suspensions of AuNPs between 10 and 50 nm display a brilliant-red color and characteristically absorb light in the visible region.[8] Significantly, the wavelength at which absorption peaks is altered by interactions among the particles. Decreasing the distance between AuNPs causes a visible color change from red to blue as the absorption peak broadens and shifts toward longer wavelengths.[9−11] Therefore, in a bioassay, protein binding partners immobilized on separate particles and then mixed together signal the binding event by bringing the particles into close proximity, which induces the color change. Assuming that one has control over the circumstances of the particle agglomeration,[12] such an assay also has the potential to be used as a versatile platform for the high-throughput screening of small-molecule inhibitors.[13,14]

Ideally, AuNP bioassays will be sensitive and specific, in addition to being reproducible. However, one of the major components of the assay, the AuNP itself, is the source of variability and irreproducibility of the assay results. While the effect of the interparticle distance on the peak absorbance wavelength has been well established,[15] the contribution of the nanoparticle diameter to the sensitivity of detecting the color change has largely been ignored. The size of the core nanoparticle is a critical factor in producing reliable results. It affects nearly every aspect of their behavior, from salt concentration tolerance[16] to the peak absorption wavelength.[17] In fact, the extinction coefficient of AuNPs increases exponentially with the diameter.[12] Therefore, a lower concentration of large particles is sufficient to achieve useful color intensity compared to smaller particles. Thus, larger AuNPs are desirable to increase the sensitivity of bioassays because fewer interactions

Received: April 12, 2011
Accepted: June 23, 2011
Published: June 23, 2011

are required to generate a detectable change of the solution color.

AuNPs are commonly synthesized by the Turkevich method,[18] which generates nanoparticles with variable diameters (10−100 nm) depending on the amount of citrate used in the process. Unfortunately, large nanoparticles produced by the Turkevich method display a broad distribution of diameters (polydispersity),[19] both within a batch and between batches. The inconsistent nanoparticle size is a problem because the same color change is produced whether it is generated by many interactions among small nanoparticles or a few interactions among large nanoparticles. Therefore, in order to obtain reproducible results and to enable comparisons among different researchers, it is imperative to be able to reliably produce AuNPs of optimal size with minimal polydispersity.

The second important consideration in the development of a reliable nanoparticle assay for detecting protein−protein interactions is the method of protein attachment. In many published studies, proteins have been nonspecifically adsorbed onto AuNPs and then used as molecular probes in binding assays.[20] The problem is that nonspecifically bound proteins can easily dissociate, which will expose charges on the particles.[21] Exposed surface charges induce particle aggregation and make it impossible to distinguish between color changes caused by a specific and a nonspecific interaction. Similarly, the nonspecific adsorption of probe proteins presents the molecules in a random orientation, decreasing the chance of exposing the binding site and therefore decreasing the sensitivity of the assay.

Thus, it is clear that currently available methods for large nanoparticle synthesis and for optimal presentation of the proteins of interest need to be optimized in order to create reproducible and reliable AuNP assays with commercial applications.

Here we present optimized methods to (1) synthesize homogenous populations of large AuNPs and (2) apply heterologous nitrilotriacetic acid−nickel self-assembled monolayers (NTA-Ni-SAMs) to the nanoparticle surface for controlled protein presentation. We show that SAM coatings render the nanoparticles resistant to self-aggregation and provide stability over a wide range of salt concentrations, pHs, and temperature conditions. Our methods were proven to be the foundation for the design of a reproducible and reliable binding assay by significantly decreasing the nonspecific binding and increasing the signal strength, thereby enhancing both the sensitivity and specificity. Finally, we are convinced that our assay can be used for the development of high-throughput small-molecule screening assays to identify drugs with the potential of inhibiting specific interactions involved in the development of cancer or other diseases and life-threatening conditions.

MATERIALS AND METHODS

AuNP Synthesis. AuNPs were synthesis by adding a sodium citrate solution (up to 25 mol equiv) to a boiling $HAuCl_4 \cdot 3H_2O$ solution (38.1 μM) with constant stirring for 30 min (see the Supporting Information). Size analysis of the nanoparticles was performed by transmission electron microscopy (TEM) on a JEOL 1200ex microscope (Harvard Medical School, Boston, MA).

Dynamic Light Scattering (DLS) Measurements. The hydrodynamic radius (Rh) of AuNPs (15−30 nm) was measured using a Viscotek 802 DLS instrument (Viscotek, Houston, TX) at 20 °C. Each DLS experiment consisted of 60 runs of 5 s each. *OmniSIZE 3.0* software was used to calculate the hydrodynamic radius of the particles based on the correlation function obtained from DLS measurements (see the Supporting Information).

Synthesis and Deposition of SAM Components. The disulfide of mercaptoundecanoic acid was purchased from Sigma-Aldrich. The triethylene glycol (EG3) and nitrilotriacetic acid (NTA) terminated thiols were synthesized according to published methods[22−24] and matched published NMR shifts. The SAM was formed according to previously published methods.[13,14]

Nanoparticle Salt Stress Assay. Nanoparticle batches of known average diameters (from 13 to 31 nm) were either unmodified, coated with an NTA-SAM, or incubated with 0.01% Tween 20 before being mixed with an equal volume of a NaCl solution (from 100 to 2000 mM). The picture was taken after 1 h of incubation (see the Supporting Information).

Nanoparticle pH Stress Assays. AuNPs of 25 nm diameter were either unmodified or coated with a NTA-SAM and resuspended in buffers of different pHs (from 2 to 10). The nanoparticles were incubated for 1 h at room temperature and then subjected to a salt stress assay, as described above. The picture was taken after 1 h of incubation (see the Supporting Information).

Peptide and Protein Attachment. AuNPs (25 nm) were either unmodified or coated with a NTA-SAM and activated with a solution of $NiSO_4$ (0.001%). The AuNPs were incubated at room temperature for 5 min, washed, and resuspended in a 10 mM phosphate buffer (pH 7.4), 140 mM NaCl, and 0.01% Tween 20. AuNPs were then loaded with either of the following peptides: (1) MUC1* peptide (GTINVHDVETQFNQYKTEAASRYNLTISDVSVSDVPFPFSAQSGAHHHHHH), (2) irrelevant GSD peptide (GGDVGDSGGDVGDSGGDVGDSHHHHHH), or (3) irrelevant RDG peptide (HHHHHHSSSSGSSSSGSSSSGGRGDSGRGDS). Histidine-tagged SNAP25 and Syntaxin1a (Abcam, Cambridge, MA) were also used (see the Supporting Information).

Antibody-Induced Agglomeration Assay #1 (Antibody Specificity). Bare and NTA-Ni-SAM-coated AuNPs (25 nm) were either unmodified or loaded with the MUC1* peptide (250 and 500 nM). The samples were incubated at room temperature for 10 min. Anti-GFP antibody (Santa Cruz Biotechnology, Santa Cruz, CA) and anti-MUC1* antibody (Minerva Biotechnologies, Waltham, MA[25]) were then added to final concentrations of 0, 67, and 134 nM. The picture was taken after 1 h of incubation (see the Supporting Information).

Antibody-Induced Agglomeration Assay #2 (Peptide Specificity). NTA-Ni-SAM-coated AuNPs (25 nm) were loaded with either 250 nM MUC1* peptide or 250 nM irrelevant GSD peptide. Anti-MUC1* antibody was then added to final concentrations of 0, 5, 10, 20, 50, and 100 nM. The picture was taken after 1 h of incubation (see the Supporting Information).

SNAP25 and Syntaxin1a Binding Assay. NTA-Ni-SAM-coated AuNPs were separately loaded with histidine-tagged SNAP25 or histidine-tagged Syntaxin1a (Abcam, Cambridge, MA) to a final concentration of 1 μM using the same method as that described above. The plate was allowed to incubate at room temperature for 10 min. Then, AuNPs were mixed together and incubated at room temperature for 2 and 10 min (see the Supporting Information).

Nanoparticle Size Sensitivity Assay. NTA-Ni-SAM-coated AuNPs of sizes 15, 20, 25, 30, and 35 nm were loaded with MUC1* as described above. Anti-MUC1* antibody (α-MUC1*) was then added to final concentrations of nanoparticles of 0, 0.67, 3.33, 6.67, 10.0, 13.3, 20.0, and 33.3 nM α-MUC1* (see the Supporting Information). Spectral measurements were taken on a Tecan Spectra Rainbow (Tecan, Durham, NC). A photograph was taken at 2 h. The relative aggregation was measured via a change in absorbance at 521 nm because this measurement reflected aggregation and precipitation. The percent aggregation was calculated using eq 1, where A_{521} at t_∞ is the absorbance at 521 nm after

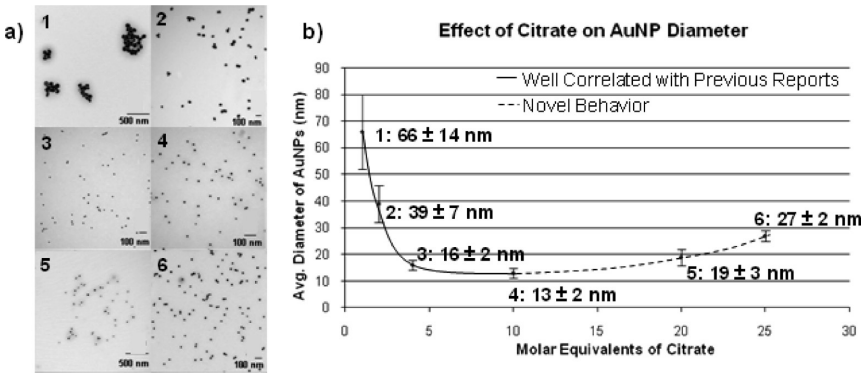

Figure 1. Novel synthesis of AuNPs. The problem of polydispersity in the synthesis of large-diameter nanoparticles is solved when gold salts are boiled in very high concentrations of sodium citrate. (a) The effect of sodium citrate on the nanoparticle diameter reverses at very high citrate concentrations. AuNPs were produced by the Turkevich method except that the concentration of sodium citrate was increased well beyond what had previously been tested. TEM was used to measure the diameter of the nanoparticles produced at various concentrations of sodium citrate. The standard deviation represents the polydispersity of the diameter within a batch. (b) At greater than 10 mol equiv of sodium citrate to gold salt, the nanoparticle diameter begins to increase rather than decrease without increasing the polydispersity. The diameter of AuNPs measured by TEM was plotted as a function of the citrate concentration used in that batch. The solid trace corresponds to previous reports that the nanoparticle diameter decreases as the citrate concentration increases. The dashed trace showing the nanoparticle diameter increasing at very high citrate concentrations is previously unreported novel behavior.

a 24 h incubation period of a fully precipitated sample and thus represents maximal aggregation (see the Supporting Information):

$$K = \frac{A_{521}^{t} - A_{521}^{t_0}}{A_{521}^{t_\infty} - A_{521}^{t_0}} \times 100 \quad (1)$$

Nanoparticle Temperature Stress Assay. NTA-Ni-SAM-coated AuNPs (25 nm) were maintained at either ambient temperature or 37, 55, or 80 °C, and a sample was removed after 30 min and 1, 2, 4, and 6 h, cooled down, and loaded with $NiSO_4$ and MUC1* peptide (500 nM) as described above. Anti-MUC1* antibody or anti-GFP antibody was then added to a final concentration of 64 nM. Photographs were taken after 30 min of incubation (see the Supporting Information).

Nanoparticle Freeze−Thaw and Lyophilization Assay. Bare AuNPs containing 0.01% Tween 20 and NTA-SAM-coated AuNPs were independently kept at 4 °C, frozen at −70 °C for 2 h and then thawed, or freeze-dried and then reconstituted. All batches were loaded with $NiSO_4$ and MUC1* peptide, as described above, and either anti-MUC1* antibody, anti-MUC1* Fab fragment, or irrelevant anti-GFP antibody was added. A photograph was taken at 1 h of incubation (see the Supporting Information).

Lyophilization of Peptide-Loaded AuNPs. NTA-Ni-SAM-coated AuNPs were loaded with MUC1* peptide, as described above, frozen, lyophilized, and then reconstituted and subjected to antibody-cross-linking with either anti-MUC1* antibody or irrelevant anti-GFP antibody (see the Supporting Information).

High-Throughput Drug Screening. NTA-Ni-SAM-coated AuNPs were incubated with a 10 μM MUC1* peptide solution or a 10 μM irrelevant RGD peptide solution. Freshly prepared T47D (ATCC) cell lysate (containing MUC1* dimerizing ligand NM23) was then added in the presence of 5 μL of phosphate-buffered saline (PBS; pH 7.4) or 5 μL of a compound (1 mg/mL in dimethyl sulfoxide) from a drug-screening library (Comgenex). AuNPs were mixed and incubated at room temperature for 10 min (see the Supporting Information).

RESULTS

Nanoparticle Synthesis. We have modified the traditional Turkevich method to synthesize AuNPs of homogenous diameter in the 20−30 nm range. In a standard protocol, AuNPs are produced when gold salts ($HAuCl_4$) are boiled in a sodium citrate solution.[18] On the basis of this method, we generated a series of nanoparticles by systematically increasing the ratio of sodium citrate to $HAuCl_4$ and then measured the mean nanoparticle diameter of each batch by TEM (Figure 1a). Increasing the amount of sodium citrate is known to reduce the particle diameter (Figure 1b, solid line).[26,27] However, we show for the first time that when the amount of citrate is increased beyond 10 equiv, the nanoparticle diameter increases, rather than decreases, albeit at a much slower rate (Figure 1b, dashed line). The gradual increase in the diameter, as a function of the citrate concentration, has the great advantage of significantly reducing the polydispersity of the particle size in the final product and increasing the reproducibility (Figure 1a).

SAM Coatings of AuNPs. We next investigated the effects of SAM coatings on the AuNP stability, under various conditions. Because sulfur binds to gold,[28] alkanethiols, under the right conditions, should form SAMs on AuNPs. Early studies aimed at functionalizing AuNPs with alkanethiols employed a method wherein thiols were present during synthesis of the nanoparticle itself.[29−34] Although these methods yielded thiol-derivatized nanoparticles, the method limits the size of the nanoparticles to the 2−5 nm range.[6] Others, using homogeneous populations of thiols, functionalized larger AuNPs (25−40 nm) by depositing thiols in highly aqueous solutions.[35] However, both the method of SAM formation and the nature of the headgroup itself, through steric hindrance or charge repulsion, appears to have prevented complete monolayer coverage. For example, the number of fluorescein-labeled DNA-terminated thiols that deposited on 15.7 nm AuNPs was measured to be 37 pmol/cm^2.[36] This is approximately 20 times less than the theoretical number required for complete monolayer coverage, which is about 770 pmol/cm^2 [assuming roughly a Au(111) surface].[37]

We developed a novel protocol for forming SAMs on nanoparticles in which mixed species of thiols, including a charged species, are initially deposited onto AuNPs from an organic solvent. Defect sites that cause nanoparticle instability and give rise to nonspecific binding are filled in with EG3-terminated

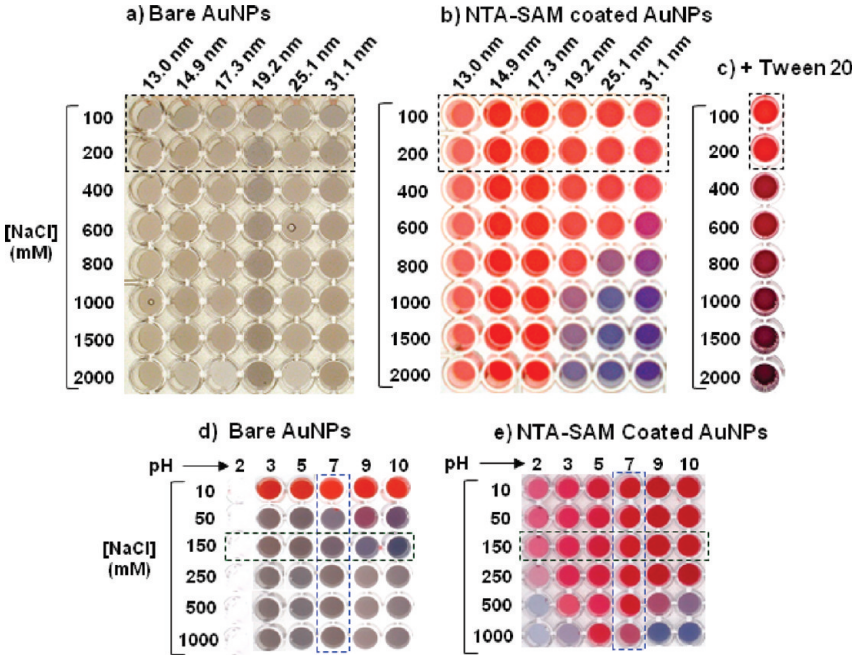

Figure 2. Stability of bare versus NTA-SAM-coated nanoparticles. NTA-SAMs render AuNPs of various sizes stable over a wide range of salt concentrations and pHs. (a and b) Salts mask surface charges on AuNPs, which causes them to aggregate and makes the solution color change from red to blue-gray. AuNPs from 13 to 31 nm in diameter that were either bare or coated with NTA-SAMs were incubated in various concentrations of NaCl as indicated. Resistance to salt-induced aggregation was determined by observing the solution color change after 1 h. (c) Small amounts of detergent make bare AuNPs resist salt-induced aggregation. AuNPs of 25 nm diameter were incubated in solutions of the indicated salt concentration that also contained 0.01% Tween 20. Dashed boxes indicate physiological salt concentrations. (d and e) NTA-SAMs make AuNPs stable at physiological pH and salt concentrations. AuNPs of 25 nm diameter were incubated for 1 h in solutions containing the indicated concentration of NaCl and at the indicated pH. Dashed boxes represent physiological NaCl concentrations and the pH.

thiols in a second step involving a heat cycling step.[13,14] Thus, complex, heterologous SAMs were formed on AuNPs that contain (1) NTA thiols, charged with Ni for the controlled capture and optimal presentation of histidine-tagged proteins or peptides,[22,23] (2) EG3-terminated thiols for the minimization of nonspecific binding,[24] and (3) carboxy-terminated disulfides for the prevention of inherent charge-induced particle aggregation.

We first tested the ability of SAMs to stabilize AuNPs in salt-containing solutions. Nanoparticles with diameters from 13 to 31 nm were incubated in NaCl solutions (from 100 to 2000 mM), and particle aggregation, that is, stability, was followed over time. Bare AuNPs, regardless of their diameter size, precipitated from solution at all salt concentrations tested (Figure 2a). In contrast, SAM-coated nanoparticles of all sizes were stable at physiological salt concentrations (100−200 mM), while particles with diameters greater than 19 nm precipitated at very high salt concentrations (Figure 2b). Interestingly, the presence of a small amount of Tween 20 increased the stability of bare AuNPs (Figure 2c), and the nanoparticle diameter had no effect on this phenomenon (data not shown).

Finally, we tested the ability of SAM-coated nanoparticles to resist pH-induced precipitation. Figure 2d shows that none of the bare AuNPs were stable at any pH tested. However, the SAM coating provides nanoparticle stability over a wide range of pHs at physiologically relevant salt concentrations (Figure 2e).

Detection of Protein−Protein Interactions. Thus far, we have only compared the stability of SAM-coated AuNPs to bare AuNPs. It could be argued that probe proteins that are non-specifically adsorbed onto AuNPs protect the nanoparticle from salt- or pH-induced precipitation while presenting the probe molecule for subsequent interaction assays. Therefore, we attached a histidine-tagged peptide to either NTA-Ni-SAM-coated or bare AuNPs and then compared their ability to participate in a specific interaction. Loading of the peptide was confirmed by western blot. A histidine-tagged MUC1* peptide was either added to NTA-Ni-SAM-coated AuNPs or nonspecifically adsorbed onto bare AuNPs in the presence of a small amount of detergent. Absorbance plots of the nanoparticles before and after coating with the SAM and subsequent loading of the peptide revealed a small decrease in absorbance around 520 nm. There was no measurable shift in the absorbance curve between conditions or a difference between SAM-coated AuNPs or peptide-loaded SAM-coated AuNPs (see Figure S1 in the Supporting Information). The cognate antibody (raised against the MUC1* peptide)[25] or a control antibody (anti-GFP) was then added to each set of peptide-bearing nanoparticles. Because antibodies are bivalent, the simultaneous binding of a single antibody to antigens on different nanoparticles brings the particles together and causes a color change from red to blue-gray. The addition of anti-MUC1* antibodies to the MUC1* peptide-bearing SAM-coated AuNPs induced a red-to-gray color change, while the irrelevant antibody induced no color change even after hours (Figure 3a, right panel). In sharp contrast, neither the cognate antibody nor the irrelevant antibody induced a color change when added to the bare nanoparticles onto which the MUC1* peptide had been nonspecifically adsorbed (Figure 3a, left panel).

In a parallel experiment, an irrelevant peptide was used as a control. Two sets of NTA-Ni-SAM-coated AuNPs were loaded with either the histidine-tagged MUC1* peptide or a

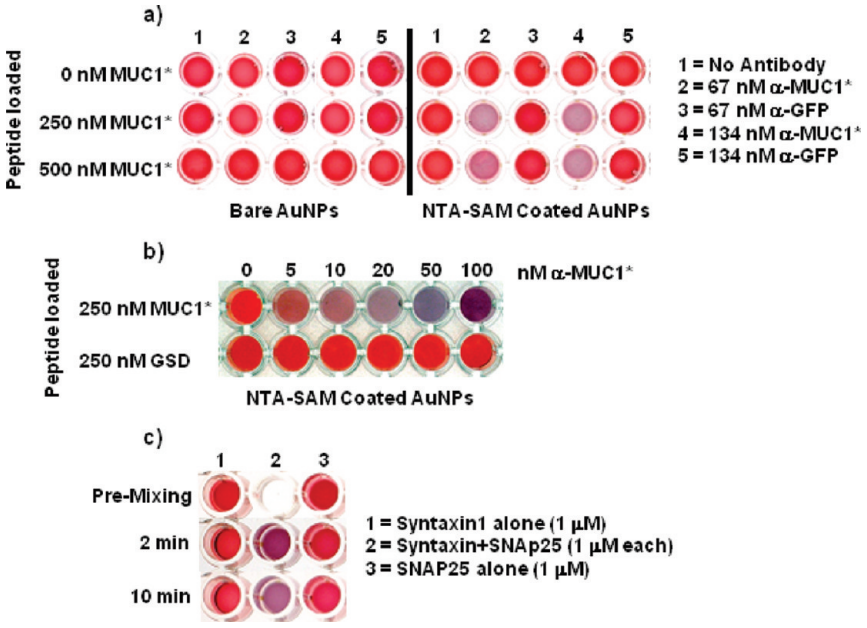

Figure 3. Protein−protein interaction assay. Protein−protein interactions are easily detected when probes are loaded onto NTA-SAM-coated AuNPs but undetectable when nonspecifically adsorbed onto bare AuNPs. (a) The color of AuNPs changes from red to blue-gray as the distance between nanoparticles is reduced, for example, when peptides on nanoparticles interact with each other or with a common target. Bare and NTA-SAM-coated AuNPs were loaded with three concentrations of a histidine-tagged MUC1* peptide and then exposed to either the cognate antibody (α-MUC1*) or an irrelevant control antibody (α-GFP). When the MUC1* peptides immobilized on NTA-SAM-coated AuNPs were exposed to α-MUC1*, the solution color changed from red to blue-gray, indicating an interaction, but not when they were exposed to the control antibody. There was no color change for any of the wells in which the MUC1* peptide had been nonspecifically adsorbed onto bare AuNPs. (b) The solution color change is the result of a specific protein−protein interaction. NTA-SAM-coated AuNPs were loaded with either the histidine-tagged MUC1* peptide or a histidine-tagged control peptide (GSD) and exposed to increasing concentrations of anti-MUC1*. The incubation of the MUC1* peptide and α-MUC1* resulted in a solution color change but not incubation of the antibody with the control peptide, indicating that the color change is due to specific interaction between binding pairs. (c) Interaction of protein binding partners separately immobilized onto different sets of NTA-SAM-coated nanoparticles is readily detected when nanoparticles are mixed. Two separate sets of NTA-SAM-coated AuNPs were loaded with equal concentrations of either histidine-tagged SNAP25 or histidine-tagged Syntaxin1a. The two nanoparticle solutions were mixed together, and a color change indicating their interaction was observed within 2 min.

histidine-tagged control peptide (GSD). Both sets were exposed to our anti-MUC1* antibody. Only NTA-Ni-SAM-coated AuNPs presenting the histidine-tagged MUC1* peptide were cross-linked by the addition of the cognate antibody and displayed a dose-dependent color change (Figure 3B).

Finally, we tested the versatility of the NTA-Ni-SAM-coated AuNP platform as a method to analyze protein−protein binding using the well-known binding pair SNAP25/Syntaxin1a.[38] The histidine-tagged proteins were loaded onto separate batches of nanoparticles and then mixed together in equal volumes. As seen before, the specific heterodimer formed by the two proteins yields a cross-linking-dependent color change (Figure 3c, column 2). No change in color was observed when the individual proteins where incubated alone (Figure 3c, columns 1 and 3).

Sensitivity as a Function of the Nanoparticle Size. Designing a AuNP bioassay to be as versatile as possible requires a system that produces reliable color changes even at protein concentrations in the nanomolar range, which is physiologically relevant. While the optical properties of AuNPs in the range of 10−40 nm are theoretically excellent for color-change assays, it became clear that the larger particles offered a much lower detection limit (Figure 4). Subjecting MUC1*-loaded AuNPs to the cognate antibody ranging from 3.3 to 33 nM displayed an unambiguous relationship between the size and detection limits. The 15 nm AuNPs displayed no aggregation at all, while the 35 nm nanoparticles displayed measurable aggregation as low as 6.7 nM α-MUC1* (Figure 4a,b). Additionally, DLS analysis in the presence of 33.3 nM α-MUC1* clearly shows the presence of large, multiparticle aggregates in solutions of large AuNPs (25 and 30 nm; Figure 4c).

Investigation of SAM-Coated AuNP Stability for Their Use in Bioassays. The structural integrity of the SAM itself, in response to various stressors, is an important consideration for the adoption of a particular nanoparticle platform. A typical method for assessing the robustness of a product and estimating its shelf-life is to test for its function after exposure to elevated temperatures. An even more stringent test is to evaluate its function after freeze−thaw or freeze-dried cycles. We therefore investigated the effect of prolonged exposure to elevated temperatures on the SAM-coated AuNPs' ability to perform reproducibly in subsequent assays. NTA-Ni-SAM-coated AuNPs were first incubated at varying temperatures for increasing lengths of time. They were then loaded with the histidine-tagged MUC1* peptide and subjected to an antibody cross-linking assay. Figure 5a shows that SAM-coated AuNPs are stable over a range of temperatures, and even exposure to 80 °C for up to 6 h did not disrupt the SAM or adversely affect its properties.

Freezing and lyophilization are excellent methods for preserving many biological molecules and also provide commercial advantages such as extended shelf-life and ease of shipping. Separate sets of either bare or NTA-Ni-SAM-coated AuNPs were either refrigerated, frozen, or lyophilized and

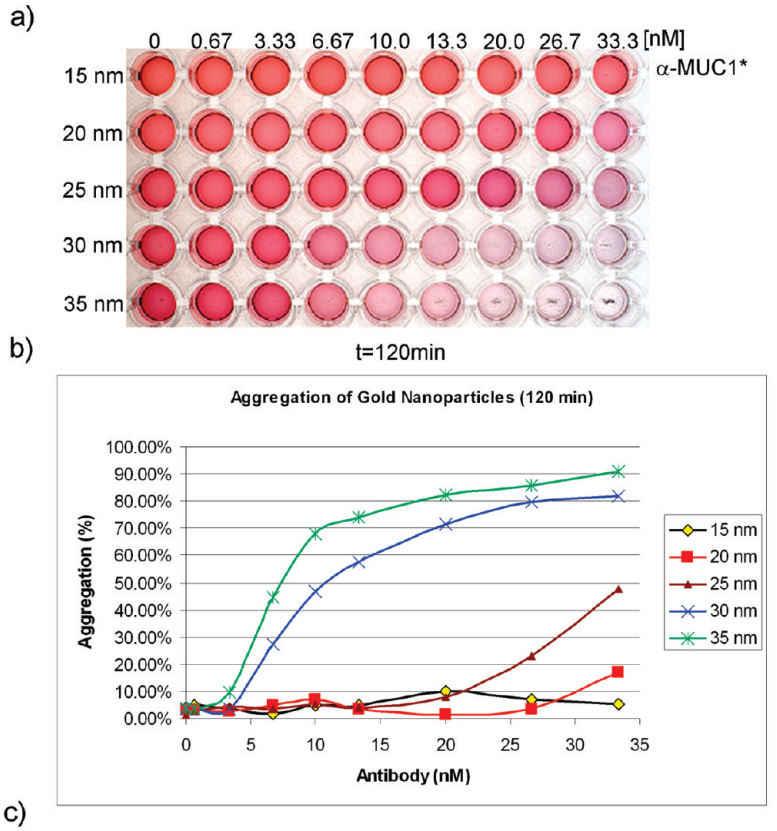

c)

DLS Size Analysis	15 nm	20 nm	25 nm	30 nm
bare AuNP*	26.2	29.4	30.2	33.6
+ SAM*	20.2	23.6	26.0	30.8
+ MUC1*	22.2	26.6	30.2	35.4
+ α-MUC1* (33 nM)	37.8 (42.6%)	48.8 (65.6%)	78 (21.9%)	75.2 (20.3%)
	74.4 (55.8%)	116.0 (31.2%)	291.8 (77.8%)	308.6 (71.8%)

Figure 4. Correlation between the nanoparticle size and sensitivity. The size of AuNPs in solution heavily influences the sensitivity of the assay to target-induced aggregation. (a) Larger nanoparticles (25−35 nm) are visually more sensitive to detecting antibody-induced aggregation, with the 30 and 35 nm AuNPs capable of detecting interaction with the α-MUC1* antibody down to 6.7 nM. (b) The calculated percentage of aggregation (see the Supporting Information) after 120 min is plotted as a function of the antibody concentration. (c) DLS measurements. The hydrodynamic radius was used to calculate the particles size in nanometers. The size of the particles decreases after SAM deposition (+SAM) and then increases after loading of the MUC1* peptide (+MUC1*). After 30 min of incubation with α-MUC1* at 33 nM, 15 and 20 nm AuNPs show a mixed population of antibody-saturated single particles (one particle + ∼12 nm from antibodies) and biparticles (two particles linked by α-MUC1*). However, 25 and 30 nm AuNPs show more than 70% larger aggregates (between seven and nine particles).

then reconstituted and loaded with the histidine-tagged MUC1* peptide, after which they were tested for their ability to perform in a specific binding assay. Figure 5b shows that NTA-Ni-SAM-coated AuNPs performed comparably whether fresh, previously frozen, or lyophilized, while bare nanoparticles irreversibly aggregated when lyophilized. Regardless of the storage method, the cognate antibody induced cross-linking of NTA-Ni-SAM-coated AuNPs loaded with the histidine-tagged MUC1* peptide, which was inhibited by the addition of the Fab of the same antibody. No color change resulted from the incubation of stable bare nanoparticles with either antibody or Fab.

In an extension of this experiment, NTA-Ni-SAM-coated AuNPs were first preloaded with the MUC1* peptide prior to lyophilization. After reconstitution with water, these particles were then treated with the anti-MUC1* antibody or an irrelevant anti-GFP antibody. Only the particles exposed to the cognate antibody exhibited a cross-linking-induced color change, while the particles exposed to irrelevant antibody demonstrated no color change (Figure 5c).

High-Throughput Drug Screening. Finally, we exploited our system for its potential to identify inhibitors of protein−protein binding. A high-throughput drug screening assay was performed with a small-molecule library. Individual small molecules were added to NTA-Ni-SAM nanoparticles bearing the MUC1* peptide, followed by the addition of breast cancer cell line T47D lysate (containing MUC1*'s ligand NM23, which binds as a dimer[25]). Figure 6 shows a representative plate screened from the library of compounds. Positive controls show a blue-gray color, which represents the specific MUC1*−ligand interaction, while the negative controls, in which an irrelevant peptide is immobilized on the

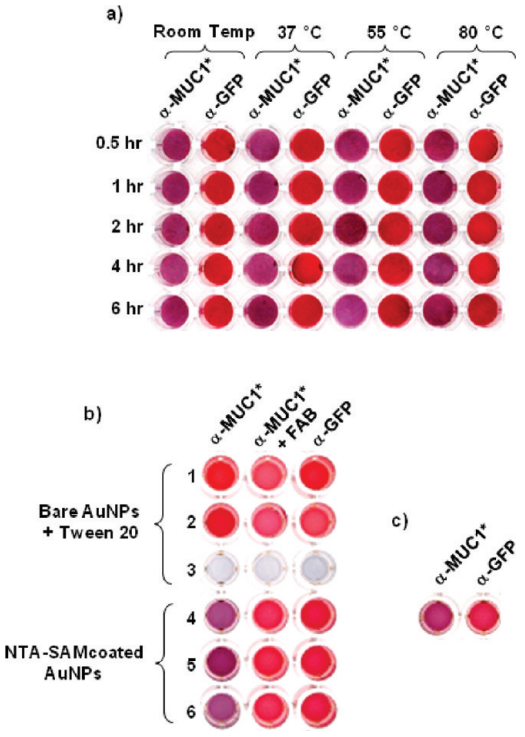

Figure 5. Nanoparticle stability and storage. NTA-SAM-coated AuNPs are not damaged by prolonged exposure to elevated temperatures, freezing, or lyophilization and can be preloaded with peptide prior to storage. (a) The performance of NTA-SAM-coated nanoparticles is unchanged after exposure to temperatures as high as 80 °C for up to 6 h. NTA-SAM-coated AuNPs in solution were held at either room temperature or 37, 55, or 80 °C for the amounts of time indicated and then tested for their ability to perform in a protein binding assay. The nanoparticles were loaded with the histidine-tagged MUC1* peptide and tested for specific aggregation in the presence of either the cognate antibody (α-MUC1*) or an irrelevant control antibody (α-GFP). The solution color changed, indicating specific interaction of the MUC1* peptide with anti-MUC1*. (b) NTA-SAM-coated AuNPs are amenable to long-term storage. Bare and NTA-SAM-coated AuNPs were subjected to three storage methods before being coated with the histidine-tagged MUC1* peptide and tested for specific aggregation in the presence of either the cognate or irrelevant control antibody: refrigeration (rows 1 and 4), freeze−thaw (rows 2 and 5), or lyophilization−rehydration (rows 3 and 6). SAM-coated AuNPs but not bare AuNPs were able to perform in protein binding assays after treatment. Peptides immobilized on NTA-SAM AuNPs bound to their cognate antibody in solution, causing nanoparticle cross-linking and resulting in the expected solution color change, which was inhibited when the Fab of the antibody was added. (c) NTA-SAM-coated AuNPs can be preloaded with peptide before lyophilization for long-term storage. The histidine-tagged MUC1* peptide was loaded onto NTA-SAM-coated nanoparticles, which were then rinsed and lyophilized. After reconstitution in water, they were able to perform comparably to fresh nanoparticles. Bare AuNPs irreversibly precipitated out of the solution as soon as liquid was added to the lyophilized nanoparticles.

nanoparticles, display a clear pink color. Compared to controls, it is clear that most of the tested compounds do not inhibit the MUC1* interaction with its ligand. However, one well (C9) is clearly pink after 20 min, indicating a specific inhibition of binding. The "hit" molecule structure is shown in the inset.

DISCUSSION

Here, we exploited the intrinsic optical properties of AuNPs, coupled with our novel methods for forming SAMs to develop a reliable nanoparticle platform that is ideal for detecting protein−protein interactions. We made a crucial improvement to the Turkevich method for generating AuNPs in the 25−30 nm diameter range, which is optimal for bioassays. In the traditional Turkevich method, gold salts are boiled in a sodium citrate solution, wherein the nanoparticle diameter decreases as a function of the citrate concentration. The problem is that the slope of the particle diameter−citrate concentration curve (Figure 1b) is so steep that minor fluctuations in the citrate concentration result in large changes in the particle diameter. This severely limits reproducibility because the AuNP readout is directly proportional to the diameter of the particles. However, we discovered that when the ratio of gold salt to citrate exceeds 10 equiv, the effect reverses and the nanoparticle diameter begins to increase rather than decrease. The key feature is that the diameter increases very gradually with increasing citrate concentration. Therefore, variations in its concentration in this range have very little effect on the nanoparticle diameter.

Our hypothesis is that the increased concentration of citrate in solution acts to suppress nucleation so that gold ions reduce onto fewer nuclei, favoring the formation of larger particles. In support of this idea, we observed that the colors of the solution during our synthesis were contrary to those produced during the Turkevich method. In the Turkevich method, the solution color turns dark purple a few minutes after the addition of the sodium citrate solution to the gold salts,[27] due to the formation of very large, but loosely bound aggregates of nascent gold nuclei.[39] These aggregates later break apart as the remaining gold cations in solution are reduced onto the nuclei, which causes the solution to transition from a deep purple to the characteristic ruby-red color.

However, once we increased the ratio of citrate to gold (10−15 equiv), the initial dark-purple stage was not observed. Instead, the solution very slowly turned from completely clear to a faint pink that gradually intensified to the same ruby-red end-point color. These color changes are consistent with the idea that fewer gold nuclei originally form and their growth over time is favored.

Our novel synthesis minimizes the particle size variability both within a batch and between batches, thus greatly increasing reproducibility. Large-diameter AuNPs are generated that have less than a 10% variation in particle size (standard deviation of the mean diameter of 2 nm), which is a vast improvement over the 20% variation that the Turkevich method yields[39] (Figure 1b). In addition, this new synthesis is a practical, inexpensive, single-step process that is amenable to commercial applications. In a previously reported modification of the Turkevich method, preformed nanoparticles were added to "seed" the reaction, which produced large-diameter nanoparticles.[40] While this method does not suffer from the issue of polydispersity, it is a multistep, time-consuming process that is not commercially practical.

We also developed novel methods for forming SAMs on AuNPs, which prevents their spontaneous precipitation due to surface charges, while providing a user-friendly platform for immobilizing histidine-tagged proteins. Our SAMs make the AuNPs stable under a variety of assay conditions, including a wide range of salt concentrations, pHs, and

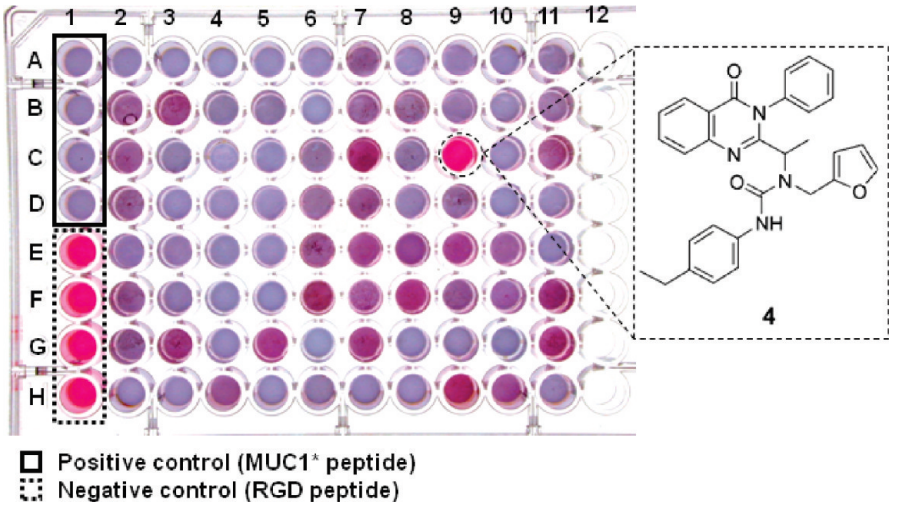

Figure 6. Small-molecule screening assay. NTA-SAM-coated AuNPs are a platform for high-throughput drug screening. A small-molecule drug library was screened for its ability to disrupt interaction between the MUC1* peptide and its ligand, dimeric NM23. All wells of a 96-well plate contain the MUC1* peptide loaded onto NTA-SAM-coated AuNPs. In column 1, rows A−D are positive controls that contain MUC1*-bearing AuNPs, while rows E−H are negative controls that contain AuNPs bearing an irrelevant peptide. All other wells contain an equal weight amount of compound of approximately the same molecular weight. The endogenous MUC1* ligand that dimerizes MUC1* (NM23) was then added to every well. The compound in well C9 inhibited the nanoparticle color change and is identified as a potent inhibitor of the MUC1*−NM23 interaction. The drug "hit" of well C9 is shown in the inset to the right.

temperatures. The SAMs are comprised of EG3- and NTA-Ni-terminated thiols, where the glycols confer resistance to nonspecific binding and the NTA-Ni moiety captures and presents histidine-tagged proteins in a controlled orientation.

In addition to traditional binding assays, we demonstrated that this nanoparticle platform is ideal for high-throughput screening of drug candidates. In fact, because of the resistance to non-specific binding that the SAM confers, drug screening can be performed in whole cell lysates. This allows one to screen for inhibitors of orphan receptors that are activated by dimerization. Using this assay, we identified small-molecule inhibitors of the oncogenic MUC1* growth factor receptor. NTA-Ni-SAM-coated nanoparticles were loaded with a histidine-tagged MUC1* peptide and incubated with cancer cell lysate suspected of containing the activating ligand. The small-molecule inhibitors identified in this assay were later directly shown to disrupt the interaction between MUC1* and its ligand, NM23, and effectively inhibit the growth of cancer cells. A statistically relevant chemophore that we identified is quinazolinone (inset, Figure 6), which has now also been identified by others as having antitumor activity.[41,42]

In conclusion, our NTA-Ni-SAM-coated AuNPs provide an ideal user-friendly platform for the study of histidine-tagged protein interaction and for identification of the agents that disrupt them. We have demonstrated the superior performance of protein and peptide binding assays performed with these SAM-coated nanoparticles over that of peptides nonspecifically adsorbed onto bare particles. For convenience, the SAM-coated nanoparticles can be lyophilized after attachment of a probe peptide and then reconstituted for later binding assays without diminution of function. Finally, the ability to detect protein−protein interaction and inhibitors thereof in a simple, one-step, colorimetric solution assay constitutes a valuable new tool for basic research as well as drug discovery efforts.

■ ASSOCIATED CONTENT

Supporting Information. Detailed methods describing nanoparticle synthesis and assay conditions. This material is available free of charge via the Internet at http://pubs.acs.org.

■ AUTHOR INFORMATION

Corresponding Author
*E-mail: cbamdad@minervabio.com.

■ ACKNOWLEDGMENT

We are grateful to Dr. Andrew Stewart for his critical reading of the manuscript.

■ REFERENCES

(1) Jeong, H.; Mason, S. P.; Barabasi, A.-L.; Oltvai, Z. *Nature* **2001**, *411*, 41–42.
(2) Stelzl, U.; Worm, U.; Lalowski, M.; Haenig, C.; Brembeck, F. H.; Goehler, H.; Stroedicke, M.; Zenkner, M.; Schoenherr, A.; Koeppen, S.; Timm, J.; Mintzlaff, S.; Abraham, C.; Bock, N.; Kietzmann, S.; Goedde, A.; Toksoz, E.; Droege, A.; Krobitsch, S.; Korn, B.; Birchmeier, W.; Lehrach, H.; Wanker, E. E. *Cell* **2005**, *122*, 957–968.
(3) Fu, H. In *Protein−Protein Interactions: Methods and Applications*; Fu, H., Ed.; Human Press: Totowa, NJ, 2004; Vol. 261.
(4) Berggard, T.; Linse, S.; James, P. *Proteomics* **2007**, *7*, 2833–2842.
(5) Shoemaker, B. A.; Panchenko, A. R. *PLoS Comput. Biol.* **2007**, *3*, e42.
(6) Daniel, M. C.; Astruc, D. *Chem. Rev.* **2004**, *104*, 293–346.
(7) Giljohann, D. A.; Seferos, D. S.; Daniel, W. L.; Massich, M. D.; Patel, P. C.; Mirkin, C. A. *Angew. Chem. Int. Ed.* **2010**, *49*, 3280–3294.
(8) van de Hulst, H. C. *Light scattering by small particles*; Wiley: New York, 1957.
(9) Dusemund, B.; Hoffmann, A.; Salzmann, T.; Kreibig, U.; Schmid, G. *Z. Phys. D* **1991**, *20*, 305–308.
(10) Kreibig, U.; Grenzel, L. *Surf. Sci.* **1985**, *156*, 678–700.

(11) Elghanian, R.; Storhoff, J. J.; Mucic, R. C.; Letsinger, R. L.; Mirkin, C. A. *Science* **1997**, *277*, 1078–1081.
(12) Nath, N.; Chilkoti, A. *Anal. Chem.* **2002**, *74*, 504–509.
(13) Bamdad, C.; Bamdad, R. S. Interaction of colloidal-immobilized species with species on non-colloidal structures. Patent Appl. PCT/US2001/020168, 1999.
(14) Bamdad, C.; Bamdad, R. S. Rapid and sensitive detection of aberrant protein aggregation in neurodegenerative disease. Patent Appl. PCT/US2000/001997, 1999.
(15) Rechberger, W.; Hohenau, A.; Leitner, A.; Krenn, J. R.; Lamprecht, B.; Aussenegg, F. R. *Opt. Commun.* **2003**, *220*, 137–141.
(16) Hiemenz, P. C.; Rajagopalan, R. *Principles of colloid and surface chemistry*, 3rd ed.; Marcel Dekker, Inc.: New York, 1997.
(17) Link, S.; El-Sayed, M. A. *J. Phys. Chem. B* **1999**, *103*, 4212–4217.
(18) Turkevich, J.; Stevenson, P. C.; Hillier, J. *Discuss. Faraday Soc.* **1951**, 55–75.
(19) Kimling, J.; Maier, M.; Okenve, B.; Kotaidis, V.; Ballot, H.; Plech, A. *J. Phys. Chem.* **2006**, *110*, 15700–15707.
(20) Glomm, W. R. *J. Dispersion Sci. Technol.* **2005**, *26*, 389–414.
(21) Brewer, S. H.; Glomm, W. R.; Johnson, M. C.; Knag, M. K.; Franzen, S. *Langmuir* **2005**, *21*, 9303–9307.
(22) Bamdad, C.; Sigal, G. B.; Strominger, J. L.; Whitesides, G. M. Molecular recognition at surfaces derivatized with self-assembled monolayers. U.S. Patent 5,620,850, Sept 26, 1994.
(23) Sigal, G. B.; Bamdad, C.; Barberis, A.; Strominger, J.; Whitesides, G. M. *Anal. Chem.* **1996**, *68*, 490–497.
(24) Pale-Grosdemange, C.; Simons, E. S.; Prime, K. L.; Whitesides, G. M. *J. Am. Chem. Soc.* **1991**, *113*, 12–20.
(25) Mahanta, S.; Fessler, S. P.; Park, J.; Bamdad, C. *PLoS One* **2008**, 3.
(26) Kumar, S.; Gandhi, K. S.; Kumar, R. *Ind. Eng. Chem. Res.* **2007**, *46*, 3128–3136.
(27) Frens, G. *Nat. Phys. Sci.* **1973**, *241*, 20–22.
(28) Nuzzo, R. G.; Allara, D. L. *J. Am. Chem. Soc.* **1983**, *105*, 4481–4483.
(29) Porter, L. A.; Ji, D.; Westcott, S. L.; Graupe, M.; Czernuszewicz, R. S.; Halas, N. J.; Lee, T. R. *Langmuir* **1998**, *14*, 7378–7386.
(30) Hostetler, M. J.; Stokes, J. J.; Murray, R. W. *Langmuir* **1996**, *12*, 3604–3612.
(31) Johnson, S. R.; Evans, S. D.; Mahon, S. W.; Ulman, A. *Langmuir* **1997**, *13*, 51–57.
(32) Evans, S. D.; Johnson, S. R.; Ringsdorf, H.; Williams, L. M.; Wolf, H. *Langmuir* **1998**, *14*, 6436–6440.
(33) Johnson, S. R.; Evans, S. D.; Brydson, R. *Langmuir* **1998**, *14*, 6639–6647.
(34) Templeton, A. C.; Hostetler, M. J.; Kraft, C. T.; Murray, R. W. *J. Am. Chem. Soc.* **1998**, *120*, 1906–1911.
(35) Weisbecker, C. S.; Merritt, M. V.; Whitesides, G. M. *Langmuir* **1996**, *12*, 3763–3772.
(36) Demers, L. M.; Mirkin, C. A.; Mucic, R. C.; Reynolds, R. A.; Letsinger, R. L.; Elghanian, R.; Viswanadham, G. *Anal. Chem.* **2000**, *72*, 5535–5541.
(37) Sellers, H.; Ulman, A.; Shnidman, Y.; Eilers, J. E. *J. Am. Chem. Soc.* **1993**, *115*, 9389–9401.
(38) Rickman, C.; Meunier, F. A.; Binz, T.; Davletov, B. *J. Biol. Chem.* **2004**, *279*, 644–651.
(39) Chow, M. K.; Zukoski, C. F. *J. Colloid Interface Sci.* **1994**, *165*, 97–109.
(40) Jana, N. R.; Gearheart, L.; Murphy, C. J. *Chem. Mater.* **2001**, *13*, 2313–2322.
(41) Bamdad, C. Compositions and methods of treatment of cancer. Patent Appl. PCT/US2002/028576, 2003.
(42) Purcell, J. W.; Davis, J.; Reddy, M.; Martin, S.; Samayoa, K.; Vo, H.; Thomsen, K.; Bean, P.; Kuo, W. L.; Ziyad, S.; Billig, J.; Feiler, H. S.; Gray, J. W.; Wood, K. W.; Cases, S. *Clin. Cancer Res.* **2010**, *16*, 566−576.